Available online at www.sciencedirect.com

ScienceDirect

Solar Energy 127 (2016) 250–261

SOLAR ENERGY

www.elsevier.com/locate/solener

# Constant temperature induced stresses in evacuated enclosures for high performance flat plate solar thermal collectors

Paul Henshall [a,*], Philip Eames [a], Farid Arya [b], Trevor Hyde [b], Roger Moss [c], Stan Shire [c]

[a] Centre for Renewable Energy Systems Technology, Loughborough University, UK
[b] School of the Built Environment, University of Ulster, UK
[c] School of Engineering, University of Warwick, UK

Received 21 September 2015; received in revised form 11 December 2015; accepted 18 January 2016
Available online 9 February 2016

Communicated by: Associate Editor Brian Norton

**Abstract**

A flat-plate solar thermal collector's efficiency can be much improved if the enclosure in which the solar absorber is housed can be evacuated. This would result in a high performance, architecturally versatile solar thermal collector capable of supplying clean energy efficiently for use in applications including residential hot water and space heating. This paper focuses on the design of evacuated enclosures for flat-plate solar collectors, in which the solar absorber is completely surrounded by a thin layer (4–10 mm) of thermally insulating vacuum, resulting in a thin solar thermal collector (depth < 20 mm). The expectations, requirements and applications of these solar collectors are discussed along with a description of the enclosure concept under consideration. Potential seal materials are identified and their limitations examined. Finite element modelling results are presented of a study investigating how the glass cover of such enclosures are mechanically stressed when subject to atmospheric pressure loading and differential thermal expansion of dissimilar components. Finite element model predictions are validated against preliminary experimental strain measurements for existing experimental enclosures. It is demonstrated that with a suitably low temperature sealing process vacuum the designed enclosure can successfully withstand imposed stresses.


*Keywords:* Renewable energy; Solar thermal; Vacuum; Stress

## 1. Introduction

Solar thermal collectors conventionally come in two forms; non-evacuated, glazed, flat plate (FP) collectors and evacuated tube (ET) collectors. FP collectors have a larger solar absorber area to gross area ratio when compared with ET collectors but their thermal performance is poorer, especially at elevated temperatures. This is due to FP collectors typically employing a solar absorbing plate (see Fig. 1) that fills a large proportion of the collector area, whilst ET collectors employ absorbing tubes which are individually enclosed in larger evacuated glass tubes. FP collectors, however, lose heat both by convection of the internal air (or gas) and conduction through it; this heat loss does not occur in a vacuum, subsequently improving the thermal performance of ET collectors. One area of research in solar thermal collectors, therefore, seeks to

*Abbreviations:* FP, flat plate; ET, evacuated tube; VFP, vacuum flat plate.

* Corresponding author. Tel.: +44 1509 635336.
*E-mail address:* p.henshall@lboro.ac.uk (P. Henshall).

http://dx.doi.org/10.1016/j.solener.2016.01.025
0038-092X/

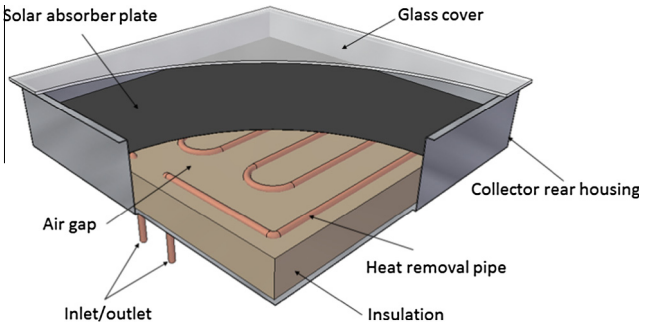


Fig. 1. Schematic diagram of a conventional flat plate solar thermal collector.

combine the benefits of ET and FP collectors (Benz and Beikircher, 1999).

Examples of successfully demonstrated low pressure flat plate solar collectors in the literature include work by Benz and Beikircher (1999), who successfully demonstrated a prototype flat plate solar collector for process steam production, with the collector interior filled with a low pressure krypton gas to reduce convective heat loss. A number of low pressure/vacuum flat plate solar collectors are starting to become commercially available, such as TVP-Solar™. It is anticipated that a vacuum flat plate (VFP) solar collector will exhibit greater efficiencies at higher temperatures in comparison to standard FP collectors and provide better use of available installation area compared to ET collectors, by capturing a greater fraction of available solar radiation. Furthermore, if the depth of flat plate systems can be reduced to 20–50 mm, increased building fabric integration is facilitated. A concept drawing of a VFP collector is presented in Fig. 2.

Fig. 2 shows a solar absorber surrounded by an evacuated volume contained by a metal housing sealed to a glass cover using a solder alloy to form a hermetic seal. Metal support pillars arranged in a regular grid pattern are positioned within the collector, allowing it to withstand atmospheric pressure forces. A series of holes in the absorber plate, allow the pillars to pass through it without making thermal contact. The absorber plate is positioned in the centre of the evacuated volume with several millimetres (4–10 mm) between it and the glass cover and rear metal housing. The collector is likely to operate at high temperatures (>100 °C) due to the thermally insulating properties of the vacuum; subsequently a thermal oil, such as Paratherm™ NF, is an appropriate working fluid to circulate within the heat removal pipes.

The mechanical design of a VFP collector has to withstand atmospheric pressure forces applied to its exterior surface. Mechanical stress in flat, rectangular, evacuated enclosures has been investigated previously for vacuum glazing applications (Fischer-Cripps et al., 1995; Simko et al., 1998; Wang et al., 2007). Vacuum glazing consists of two sheets of glass separated by an array of very small structural support pillars, typically less than 0.5 mm in both height and diameter. A seal is made around the periphery of the glass sheets and the small interior volume is evacuated to a high vacuum (less than 0.1 Pa), resulting in a narrow building component with a $U$-value less than 1 W/m$^2$ K, if low emissivity coatings are used to suppress radiative heat transfer. However, the glass sheets are subject to large, sustained stresses from atmospheric pressure loading over their surfaces and from differential thermal expansion when one glass sheet is warmer than the other.

Evacuated enclosures for flat plate solar thermal collectors have design similarities to vacuum glazing, but are subject to different design constraints and operational conditions as there are more mechanical design options. The purpose of this paper is to explore various fundamental design options and describe their effects on the mechanical stresses.

One option is for the rear glass to be replaced by a thin metal sheet. A difficulty with any evacuated flat plate

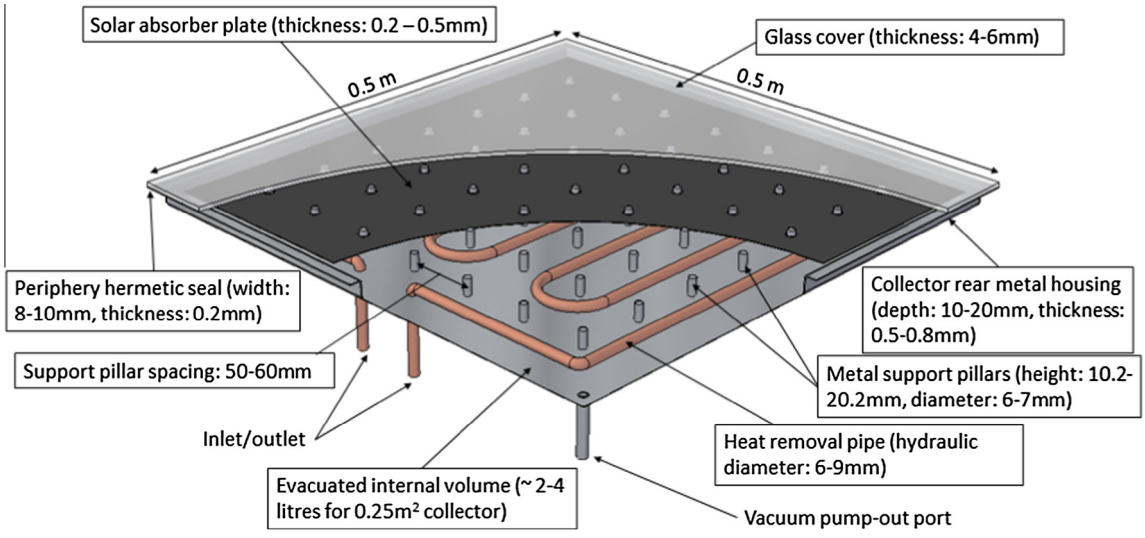


Fig. 2. Conceptual depiction of a 0.25 m$^2$ vacuum flat plate solar thermal collector.

enclosure is that the atmospheric pressure load must be divided approximately equally between the supporting pillars. When using glass front and back, any deviation from flatness will cause non-uniformity in the pillar load distribution due to the combined rigidity of the panes of glass, edge seal and pillars. This may cause reliability problems especially if one or both glass panes are tempered.

Tempered glass is stronger and safer than standard annealed glass, but due to its fabrication process is subject to the roller wave effect (Abbott and Madocks, 2001), causing its surface to undulate. The process of sealing a vacuum glazing and ensuring the support pillar array is evenly distributing mechanical stresses over the glass surface, although theoretically possible, is known to be significantly more complex when using tempered glass. This complexity most likely extends to vacuum enclosures for flat plate solar collectors with front and rear glass covers. Such an enclosure would be transparent in places, presenting an advantage architecturally, but this aside, there is no need for glass on both sides. If one side of the enclosure is fabricated from thin flexible metal, its natural flexibility might compensate for the undulating surface of the tempered glass.

Using a 3D finite element method (FEM) analysis software package (ABAQUS) a parametric study was conducted to gain understanding of the mechanical stresses expected for this evacuated enclosure concept. Mechanical stresses are predicted for (i) when the enclosure is exposed to extreme winter temperatures and (ii) different enclosure sizes. FEM models are validated against preliminary experimental measurements of enclosure strain gained using digital image correlation (DIC).

### 1.1. Background

The concept of employing an evacuated or low pressure enclosure to enhance the thermal performance of flat plate solar collectors dates back to the 1970s (Eaton and Blum, 1975). At that time flat plate solar collectors performed poorly at elevated temperatures: efficiencies were typically less than 40% for absorber plate temperatures greater than 100 °C. Eaton and Blum (1975) suggest that a moderate vacuum environment (~150–3500 Pa) between the absorber plate and enclosure glass cover will allow the collector to efficiently operate at temperatures exceeding 150 °C. Achieving temperatures of 100–150 °C would allow flat plate collectors to be considered for process heat applications.

The moderate vacuum pressure range can effectively suppress convective heat transfer between the absorber plate and the collector glass cover but does not inhibit gaseous conduction since gas conductivity is not a function of pressure. Gas conduction can account for several $W/m^2$ of total power loss from a solar collector, the exact value depending on the temperature difference between the absorber plate and glass cover (Benz and Beikircher, 1999). A vacuum pressure between the absorber plate and glass cover of less than 0.1 Pa, however, achieves a molecular mean free path in excess of the plate-to-cover spacing and effectively suppresses both convection and gas conduction processes, with a corresponding performance improvement.

Attaining and maintaining enclosure pressures below 0.1 Pa for an adequate product lifetime (20–30 years), represents a significant engineering challenge for a FP collector enclosure, especially when the vacuum layer volume is very small: in vacuum glazing the vacuum layers are typically less than 0.5 mm thick (Eames, 2008). It is essential to avoid any kind of micro-cracking, therefore the design of the evacuated enclosures must withstand the large stresses imposed by atmosphere pressure and those from differential thermal expansion between the various enclosure components.

Stress in vacuum glazing structures has been investigated extensively in the literature. Fischer-Cripps et al. (1995) utilised analytic and FEM, to characterise the magnitude of the stresses induced in vacuum glazing, whilst Simko et al. (1998) investigated how mechanical edge constraints on vacuum glazing influence the spatial distribution of stresses, when subjected to extreme temperature differentials. An experimental and theoretical study by Wang et al. (2007) explored the stresses induced in a vacuum glazing panel fabricated at low temperatures, using indium as an edge seal.

### 1.2. Configuration and performance

Conventional flat plate solar collectors are typically configured as depicted in Fig. 1. The absorber plate and heat removal tubes are insulated on the absorber's rear side and the front side has an air gap between the absorber and glass cover, often resulting in significant heat loss. In the VFP configuration (Fig. 2) the absorber plate is suspended within the housing and is completely surrounded by vacuum, suppressing convection and gas conduction heat loss. This should lead to the VFP collector operating more efficiently at higher temperatures. Moss and Shire (2014) suggests an improvement of efficiency from 25% for a conventional collector to 60–65% for a VFP collector when operating at 150 °C above ambient temperatures. Additionally, the absorber plate in a VFP collector would fill a much larger proportion of the available gross collector aperture area. Such performance enhancements suggest a VFP collector would be suitable for a range of applications such as domestic hot water/space heating and process heat production at a range of temperatures. The vacuum insulation layer surrounding the solar absorber can be very thin whilst remaining effective: no bulky backing insulation is required so the collector may be only slightly deeper than the solar absorber plate. The VFP collector could thus be more easily mounted onto existing roof structures or employed as fascia elements on buildings.

### 1.3. Hermetic sealing materials

A contiguous, robust hermetic seal between the glass cover and the collector housing maintains the vacuum within a VFP collector over its lifetime. This type of sealing is akin to that in vacuum glazing, for which there are several candidate materials (Eames, 2008). A primary consideration when selecting seal candidate materials is the softening temperature. If this in the range of 300–400 °C or higher, it is very likely that a tempered glass cover would lose temper during the sealing process (Eames, 2008). If the softening temperature of the seal material is relatively low in comparison to the stagnation temperature of the solar collector, the seal will be far more likely to fail over the product lifetime. Conventional materials considered for vacuum glazing include solder glass and indium solder alloys (Eames, 2008).

Indium solder has a softening temperature of ~154 °C and is bonded to glass and metal surfaces via ultra-sonic soldering. The sealing technique involves placing two indium coated surfaces together and baking. At this temperature the indium sub-ducts the surface oxide layer at the joint interface, resulting in a mixing of the indium and forming a seal between them. This technique works well for vacuum glazing (Eames, 2008). However, indium's low melting point poses a greater risk of seal failure for a VFP collector, especially around its inlet and outlet ports. Nonetheless, assuming the collector operation stagnation temperature is not too high and the seal is thermally insulated from the flat plate absorber, indium is a feasible seal material.

A range of tin based solders may also be considered, including S-bond 220 M, a solder alloy containing tin, titanium, silver and magnesium (S-Bond, 2015). This alloy has a softening temperature of 240–260 °C. Another tin based solder is Cerasolzer 220, with a softening temperature of around 220 °C (MBR-Electronics, 2009). The sealing technique used is similar to that for indium, however, tin based solders also require surface dross skimming and mechanical activation to break down the surface oxide layer to form the seal, further complicating the sealing process.

Wang et al. (2007) demonstrated that thermally induced glass stresses in vacuum glazing are independent of the seal material used, as long as the Young's modulus of the seal material exceeds $3.0 \times 10^9$ Pa. Indium and tin based solders have similar coefficients of thermal expansion (~25–$24 \times 10^{-6}$ $C^{-1}$) and both have Young's modulus exceeding this value, therefore the glass cover will be similarly stressed regardless of the material used. However, the thermal expansion coefficient of the glass cover is much less than these seal materials (~$9 \times 10^{-6}$ $C^{-1}$), resulting in localised tensile stress on the exterior surface of the glass cover above the seal.

### 1.4. Modelling approach

The modelling approach used in this study resembles that of Wang et al. (2007) and Simko et al. (1998) to investigate pressure and temperature induced stresses in vacuum glazing. In these cases the approach was validated against the experimental results of Simko et al. (1998) and Fischer-Cripps et al. (1995).

Stresses on the enclosure are modelled via a parametric analysis in which finite element method (FEM) software (Abaqus) is employed to model the stresses in two enclosure configurations. Each model uses 8-node linear 3D volume stress elements to model the stress behaviour of enclosure components, such as pillars, glass cover and rear metal housing, which are defined as individual deformable 3D parts. Frictional contact (friction coefficient: 0.7) between them is modelled via node-to-surface contact interaction protocols available in the Abaqus software (Fig. 4). The hermetic seal is also modelled as a separate deformable 3D part, however, a no-slip condition is enforced between the seal, the glass cover and the metal housing parts. The enclosure parts modelled in this study are listed in Table 1 along with corresponding thermal and elastic material properties:

To demonstrate the validity of the FEM models an attempt was made to reproduce some of the results published by Wang et al. (2007) and Simko et al. (1998), namely, case 1: $\sigma_{xx}$ stress profiles in the vicinity of a pillar spaced at 40 mm (Fig. 10 of Wang et al. 2007) and case 2: thermally induced strain, parallel to glazing edge, across a 500 × 500 mm vacuum glazing (Fig. 7 of Wang et al. 2007). The meshes in these analyses were refined until discrepancies between the calculated stresses and the published results were no more than 5% on average. This analysis was informed with regard to necessary minimum element dimensions and average element density of the glass cover between pillars to produce reliable and realistic stress results. The changes for the cases 1 and 2 analyses obtained with mesh refinement are plotted in Fig. 3a and b respectively. A minimum element dimension of ~0.1 mm is needed to accurately resolve peak stresses above the pillars in case 1 (Fig. 3a). Fig. 3b indicates that an average element

Table 1
FEM analysis components and material properties.

| Enclosure component | Glass cover | Support pillars | Rear housing | Hermetic seal |
|---|---|---|---|---|
| Material | Soda-lime glass | 400 series stainless steel | | Indium |
| Young's modulus | 72 GPa | 190 GPa | | 12.74 GPa |
| Poisson ratio | 0.21 | 0.29 | | 0.45 |
| Thermal expansion coefficient | 8.3 μm $m^{-1}$ $K^{-1}$ | 10.8 μm $m^{-1}$ $K^{-1}$ | | 24.8 μm $m^{-1}$ $K^{-1}$ |

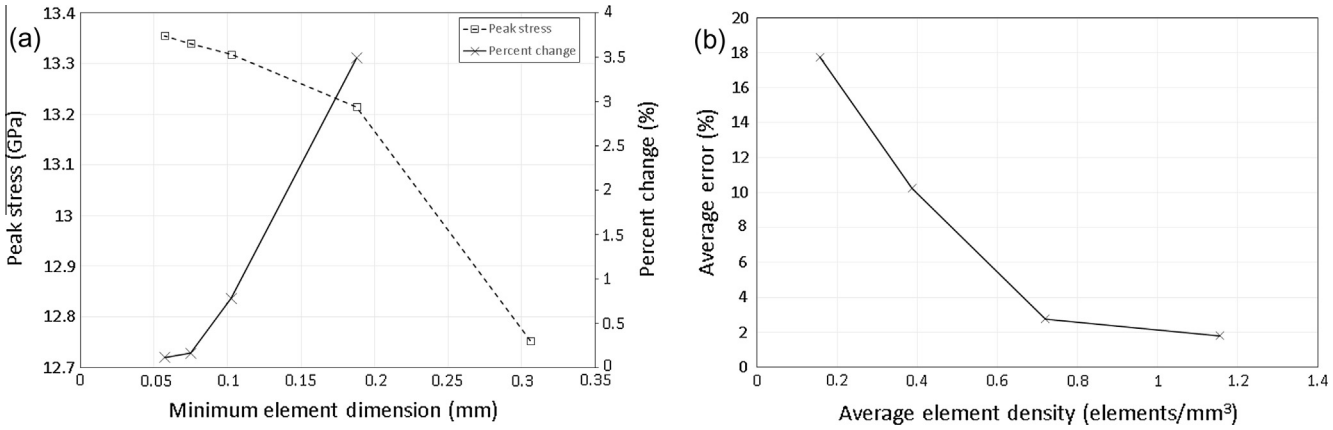


Fig. 3. Mesh refinement for (a) vacuum glazing case 1 and (b) vacuum glazing case 2.

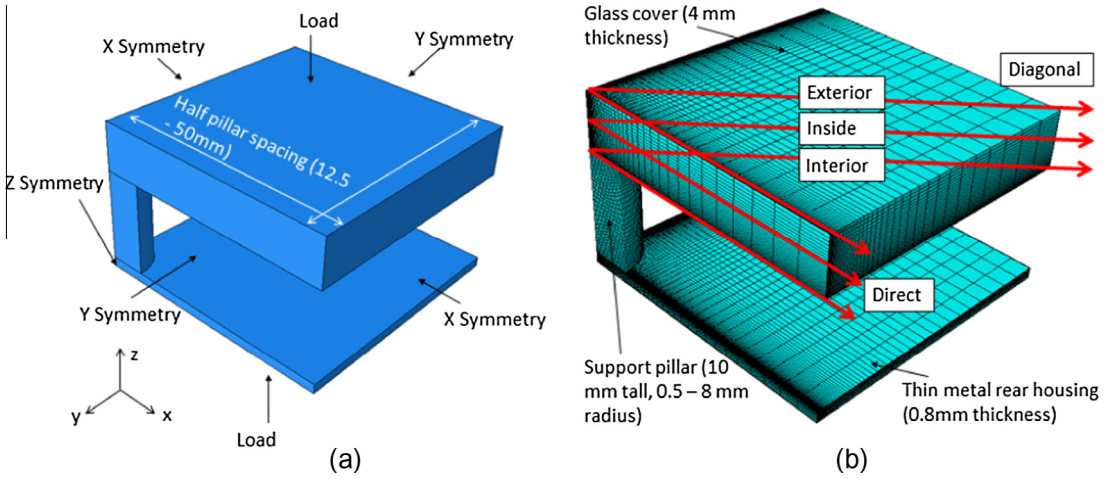


Fig. 4. Central glass cover stress (a) FEM model geometry and (b) computational mesh.

density greater than ~0.72 elements/mm$^3$ is needed to achieve average errors of less than 5% in case 2. Similar convergence studies were conducted for the FEM analyses discussed later, the results of which were consistent with the convergence of these initial analyses.

## 2. Stresses in evacuated enclosures

Although a evacuated enclosure for a flat plate solar collector is different to vacuum glazing, it is expected that, given the similar nature of the structures, a similar analysis can be conducted to assess stress resulting from atmospheric pressure loading and differential thermal expansion as was conducted previously for vacuum glazing (Simko et al., 1998).

### 2.1. Stress due to atmospheric pressure

When considering stresses induced in these enclosures due to atmospheric pressure compressing the structure, the main concern is the tensile stress induced in the exterior surface of the glass cover in the region above the support pillar contact points (Collins and Fischer-Cripps, 1991). These tensile stresses result from the air pressure loading that bends the glass into a convex shape. The deflection of the glass and collector housing between pillars is typically on the order of 0.01–0.05 mm (Wang et al., 2007), depending on pillar separation. The volume change of the enclosure when evacuated, as a result of such glass and housing deflection, is negligible (<1%), subsequently any decrease in load on the structure due to an increase in enclosure pressure as a result of the enclosure volume change is not considered.

The stresses over pillars well away from the edge seal, i.e. towards the centre of the enclosure, can be modelled by a FEM geometry, see Fig. 4a and b. The model represents one quarter of a pillar and extends over half a pillar pitch; symmetry continuation boundary conditions are applied to all four sides of the grid and an atmospheric pressure load is applied to the top and bottom surfaces. The $X$ symmetry condition sets displacements in the $x$ direction along with rotation about the $y$ and $z$ axes to zero at the boundary surface. The $Y$ symmetry and $Z$ symmetry conditions are similarly defined with the $Z$ symmetry

condition acting at just one corner point of the model. The dimensions of the support pillar and their spacing are varied systematically, to investigate the relationship between of these parameters on glass cover stress, as indicated in Fig. 4. For example, Fig. 5 shows the main principal stress on the 'exterior' and 'interior' surfaces of the glass cover as well as 'inside' the glass on its central plane for a pillar diameter of 6 mm and a pillar spacing of 60 mm. These stresses are reported along the 'direct' (horizontal or vertical) connecting line between pillars and the 'diagonal' connecting line between pillars (see Fig. 4).

As can be seen from Fig. 5 the peak principal tension stress is located directly over the top of the pillar on the exterior glass cover surface. The largest compression stress is seen on the interior glass cover surface in the vicinity of the pillar edge. It is assumed in these models that the pillar contact surface is perfectly flat which in practice will not be the case and deviations from this may lead to greater levels of stress within the glass and on the interior glass surface. Pillars manufactured for experimental testing are fabricated via a computer numerical control lathe to ensure consistent pillar size to an error of ±0.05 mm and the contact surfaces are also polished using a fine grade emery paper to smooth off any machining burs. The effect of pillar contact profiles on glass cover stresses will be investigated in a subsequent paper and it is assumed that the pillars produced for experimental testing are sufficiently flat (blunt indenter) for comparison to stress models.

### 2.1.1. Pillar array constraints

As the evacuated enclosure concept is similar to vacuum glazing configurations, many of the design constraints for vacuum glazing are transferable. These constraints include limits on: external glass cover surface tensile stress, internal glass cover stresses for the prevention of Hertzian cone fractures and compression forces on the support pillars; all of which are induced via atmospheric pressure loading. These constraints are met by careful selection of support pillar radius ($a$) and spacing ($\lambda$). A further parameter which

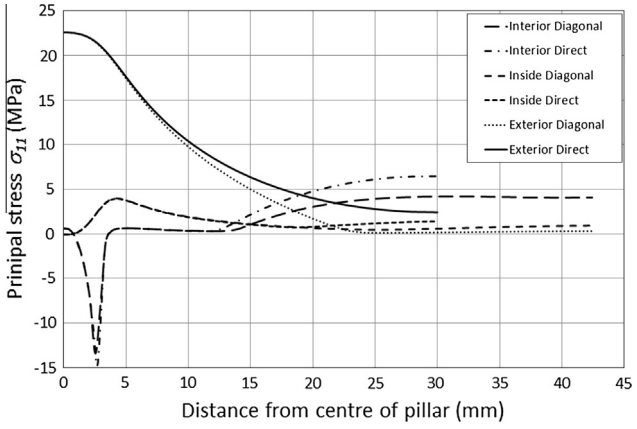


Fig. 5. Atmospheric pressure induced principal stress on 4 mm thick external glass cover surface in vicinity of 6 mm diameter support pillar for 60 mm pillar spacing.

can be varied is the glass cover's thickness, increasing the thickness will reduce the tensile stresses in the exterior surface. In this study, the glass cover thickness was kept constant at 4 mm, this being the thickness utilised in most vacuum glazing (Eames, 2008; Wang et al., 2007). The support pillar height was kept constant at 10 mm since the height of the pillar should not impact the stress experienced by the glass cover due to atmospheric pressure loading.

The first design constraint is a limit on the glass cover external stress as discussed by Collins and Fischer-Cripps (1991) for vacuum glazing. Collins and Fischer-Cripps (1991) describe the nature of the external surface tensile stresses resulting from indentation of the support pillars experienced by vacuum glazing. The external surface of the glazing is subject to abrasion through handling and weathering which can introduce flaws on the glass surface; the interior surface of the glass is not subject to such abrasion. The continual stress experienced by a vacuum glazing, over its service life of more than 20 years, can result in the growth of surface flaws to the point of failure, a process exacerbated by the presence of moisture which the external glass cover surface is exposed to, however, the interior surface is not. Collins and Fischer-Cripps (1991) examined the subcritical crack-growth behaviour of surface flaws for annealed glass immersed in water and continually stressed at 4 MPa. They determined that for a 100 year lifetime surface flaws of less than 0.35 mm would be necessary. This is roughly consistent with predictions made by Overend and Zammit (2012) when calculating failure stress for annealed glass based on similar initial flaw size and stress duration. For a evacuated flat plate solar collector a 4 MPa limit on external stress is admittedly very conservative as it is unlikely that flaw sizes greater than 0.35 mm would occur during the service life or that it would be continually wet and that the locations on the glass cover that would be stressed to this level are limited to small areas near the pillars. A 4 MPa limit constitutes an additional safety factor of 2 on top of the allowable continuous stress for annealed glass as calculated via the procedures outlined in the draft European standard prEN-13474 (European Committee for Standardisation, 2009) for a stress duration of 30 years (i.e. 8 MPa). However, the external surface of the collectors glass cover will be subject to additional sources of stress including wind and snow loading, shading stress and impact stresses from rain and hail, thus requiring additional robustness of the glass to avoid failure. Subsequently, with regard to annealed glass being used as the collectors glass cover, the 4 MPa stress constraint, as described by Collins and Fischer-Cripps (1991), was adopted in this study.

With regard to fully tempered glass, European standard EN 12150 states a characteristic bending strength of 120 MPa, using this value to calculate the allowable continuous stress for a 30 year lifetime as according to EN 13474 results in a value of ~70 MPa, thus a 35 MPa stress limit for tempered glass would incorporate an additional safety factor of 2. Schneider et al. (2012) compared the scratch

resistance of annealed and tempered architectural glass and determined that tempered glass is more sensitive to formation of scratches in comparison to annealed glass, subsequently an additional safety factor is even more important in this case along with development of appropriate collector cleaning protocols to avoid surface abrasion. In this study it is assumed that tempered glass is a valid choice for the enclosure concept and therefore the 35 MPa stress limit was selected as a design criteria. External tensile stress on the glass due to atmospheric pressure forces is determined via a parametric analysis using the computational mesh shown in Fig. 4 with a variety of pillar radii and spacing; combinations of $a$ and $\lambda$ that gave rise to external stresses of 4 MPa and 35 MPa were recorded.

The edge strength of the glass cover is dependent on the finish and quality of the glass cover edges (for example, polished or cut edges), the initial size of any flaws, the loading period and whether the glass is annealed or tempered. Different combinations of these can lead to a wide range of allowable edge stresses. For example, the edge strength of annealed, cut glass was estimated to vary depending on initial flaw size 33–300 μm, between 24 and 8 MPa respectively, as determined by the methods of Vandebroek et al. (2012) for a 30 year period. The stress on the edge of the glass cover can be reduced by allowing the glass to be slightly larger (2–3 mm) than the enclosure rear housing such that the edges are not directly loaded. Furthermore, the edges can be protected from weathering and abrasion via an appropriate protective coating, such as an epoxy. In the current analysis the edges stresses are not reported but will be discussed in subsequent papers.

The second design constraint is the formation of Hertzian cone fractures on the internal surface of the glass. These types of fracture are associated with blunt indenters (Schneider et al., 2012), such as the support pillars, and the risk of fracture formation can be found by application of Auerbach's law; based upon which Collins and Fischer-Cripps (1991) propose the following relation:

$$\lambda = 155a^{3/4} \tag{1}$$

Eq. (1) is an empirically derived relation based on extensive experimental testing conducted by both Langitan and Lawn (1969) and Mouginot and Maugis (1985) and it plots a curve for which the combinations of $a$ and $\lambda$ are just sufficient to initiate a cone fracture when glass supported by the pillar array is subject to atmospheric pressure loading. This is considered to be the primary constraint for the interior glass surface, which like vacuum glazing is expected to be stronger than the exterior surface because it is not subject to weathering or abrasion (Collins and Fischer-Cripps, 1991).

The third design constrain is with regard to the compressive stress in the support pillars themselves. The vacuum enclosure support pillar array size and spacing should be selected such that the compressive stress on the pillars does not exceed the compressive strength ($S$) of the pillar material (0.17 GPa for stainless steel). The relationship between pillar separation and pillar radius for a given compressive strength is given by:

$$q\lambda^2 \leqslant S\pi a^2 \tag{2}$$

where $q$ is the atmospheric pressure load.

A fourth constraint considers the possibility of a pillar buckling. Taking the Euler buckling load for a pin-ended column (a worst case), a buckling load constraint can be given by:

$$\frac{\pi^2 E a^4}{2L^2} \leqslant q\lambda^2 \tag{3}$$

where $E$ is the young's modulus of the pillar material and $L$ is the height of the pillar.

A final constraint identified specifically for VFP collectors is a limit on total pillar array area such that a large proportion of area is available within the vacuum enclosure for the collector absorber plate to occupy. Pillars consume aperture area that would otherwise be available for the absorber to fill in a conventional flat plate collector. The area taken up by the pillar array is a function of the total number of pillars per unit area of collector and also the diameter of each pillar. In the current study, this limit on pillar array area is set to 3% of the available area in the collector such that there should only be a 3% reduction in absorber aperture area and thus solar energy collected in comparison to a conventional flat plate collector. This criteria is approximately represented via the relation (assuming a 0.5 mm clearance between the pillars and the absorber):

$$0.03 \geqslant \frac{\pi(a + 0.5\ \text{mm})^2}{\lambda^2} \tag{4}$$

When considering all the constrains discussed above, a range of safe values for $a$ and $\lambda$ can be identified graphically using a similar procedure to Collins and Fischer-Cripps (1991). This involves plotting the curve of the combinations of $a$ and $\lambda$, derived from FEM analysis, that give rise to 4 MPa and 35 MPa external glass cover stress on a graph where values of $a$ and $\lambda$ are represented on the $x$ and $y$ axes respectively (see Fig. 6). Combinations of $a$ and $\lambda$ below these curves, respective of whether the glass is annealed or

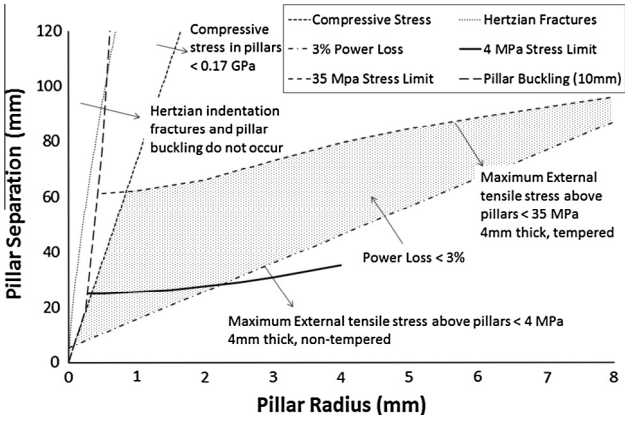


Fig. 6. Pillar array design safety envelope for 4 mm thick tempered and non-tempered glass.

tempered, results in a satisfactory combination of $a$ and $\lambda$ with regard to the first constraint. Plotting on this graph Eqs. (1)–(4) results in the other design criteria being satisfied in a similar manner and subsequently a region on the graph is defined that satisfies all design constraints.

In Fig. 6, acceptable combinations of the design parameters ($a$ and $\lambda$) can be found within the shaded region bound by the various constraint curves. From Fig. 6, maximum values of radius and spacing are found for both annealed and tempered glass. It should be noted that these analyses are representative of stresses in the centre of a 4 mm thick glass panel due only to atmospheric pressure loading. Changes in this stress level due to differential thermal expansion will be presented and discussed later.

### 2.2. Modelling and experimental considerations

Stresses are also induced in the enclosure due to differential thermal expansion of the different enclosure components. These stresses will occur when the enclosure is cooled below the solidus temperature of the sealing material used and also when the enclosure is non-uniformly heated with the glass cover being at a different average temperature to the rear metal housing. For the enclosure concept under consideration thermal expansion stresses can be visualised as seen in Fig. 7.


Fig. 7. Forces due to differential thermal expansion resulting from uniform cooling of the enclosure from the seal melting temperature and/or a temperature difference existing between the glass cover and rear metal housing.

In Fig. 7 it can be seen that there will be a finite bending moment resulting in the structure adopting a spherical shape. This is due to the different thermal expansion coefficients of the glass cover and metal tray; a similar effect is seen in vacuum glazing (Wang et al., 2007). Depending on the emissivity of the various enclosure components it is possible that the rear metal housing will be slightly cooler or warmer than the glass cover during collector operation. It is particularly important to select a metal and glass that have similar coefficients of thermal expansion.

When modelling stresses due to differential thermal expansion it is important to know the expected temperature of the enclosure. A simple worst case scenario was used to assess enclosure stresses for an enclosure sealed with a tin-based solder having a solidus temperature of 220 °C. The worst case is taken as occurring when the enclosure is cooled to a temperature of −20 °C, representative of extreme winter conditions, resulting in a 240 °C temperature difference from the stress free temperature of 220 °C. The FEM analysis models both the differential expansion and the atmospheric pressure loading, using the properties (Table 1) of 400-series stainless steel for the tray and soda-lime glass for the cover. This metal was selected due its relatively low thermal expansion coefficient, which is close to that of soda-lime glass. The dimensions of the enclosure components were based on a prototype enclosure fabricated at Loughborough University (Fig. 8a) and measuring 0.5 m × 0.5 m. In this case the glass cover thickness was 4 mm, the tray depth was 10 mm, the seal area was 10 mm and the metal tray has a thickness of 0.8 mm. The support pillars are 6 mm in diameter and spaced at 60 mm intervals. This combination of pillar size and spacing was selected as it is comfortably within the safety envelope depicted in Fig. 6 for tempered glass of this thickness. The computational mesh used for the analysis is consistent with Section 1.4. Due to symmetry considerations only a

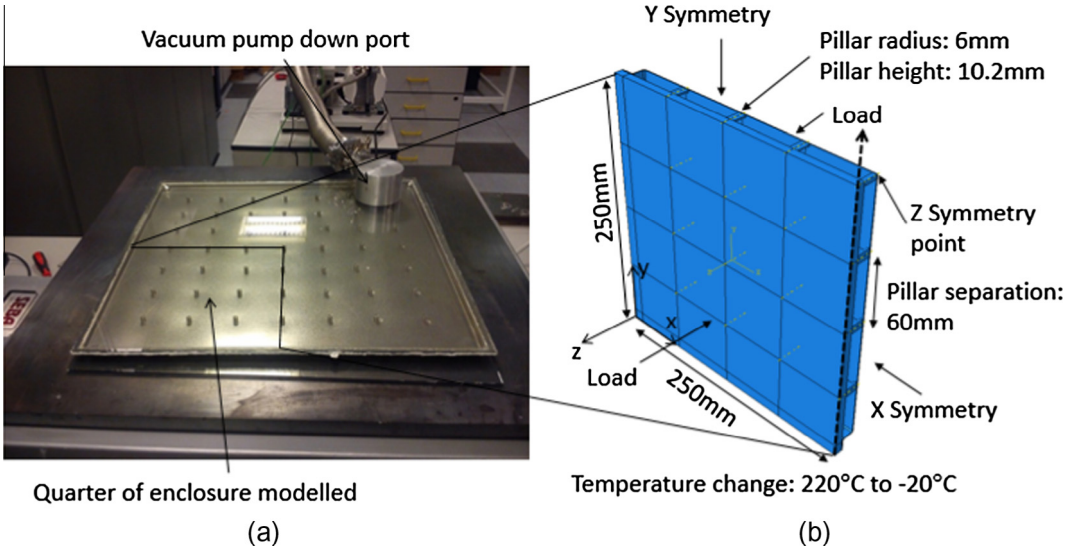


Fig. 8. (a) Fabricated 0.5 × 0.5 m metal tray enclosure; and (b) FEM metal tray enclosure quarter geometry.

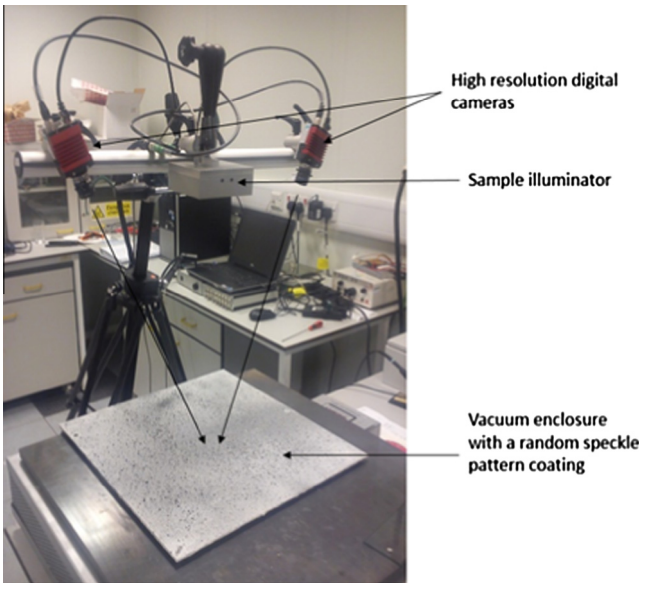


Fig. 9. DIC equipment setup for measurement of evacuated enclosure strain.

quarter of the enclosure need be modelled, this geometry is shown in Fig. 8b.

### 2.3. Digital image correlation strain measurements of the evacuated enclosure for atmospheric pressure loading

A Dantec Dynamics Q-400 DIC (digital image correlator) was used to measure the strain profile over the surface of the 0.5 × 0.5 m fabricated enclosure depicted in Fig. 8. The DIC compares images of the enclosure taken via two separate high resolution digital cameras to determine the change in strain resulting from a change in the loading conditions. The measurement requires the glass cover of the enclosure to be spray painted to produce a random black speckle pattern on a white background. The DIC system was calibrated via a standard method as outlined by Dantec and utilised standard industry image correlation parameters for the evaluation of surface principal strains (DANTEC-Dynamics, 2014). The DIC equipment setup is depicted in Fig. 9. A set of images were taken of the fabricated and sealed enclosure prior to evacuation and then again after evacuation to ~5000 Pa, which results in a pressure differential of approximately 96 kPa between inner and outer surfaces of the enclosure. Both sets of images were taken at room temperature and subsequently the DIC readings of strain show only the effects of atmospheric pressure loading. Further experiments are planned to investigate enclosure strains due to differential thermal expansion of the enclosure and will be reported in future papers.

The preliminary experiment produced principal strain contours that clearly follow the pattern of support pillars, Fig. 10.

In Fig. 10, the principal strain contours on the enclosure glass cover of Fig. 9 are seen from the aspect of one of the DIC cameras, resulting in a slightly oblique image. The black circles indicate the expected positions of the pillars underneath the glass cover, the centres of these circles do not correspond exactly with the location of the peak stress observed in the vicinity of corresponding pillars, this may be a result of slight misalignments in pillar positions and/or non-uniform contact of the pillars with the glass cover. However, similar and consistent principal strain contours were produced via a FEM simulation of the enclosure, as described in Section 2.2, in which only atmospheric pressure forces were acting on the enclosure structure, Fig. 11.

The principal strain profiles, in the vicinity of two support pillars (diagonal and direct, Fig. 10) as measured

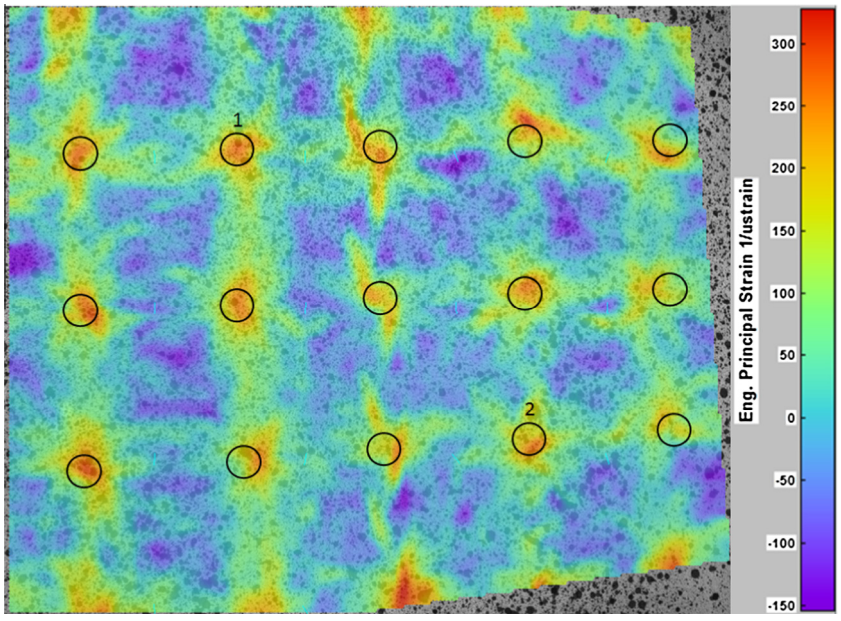


Fig. 10. DIC principal strain contours, circles indicate expected locations of pillars, strain data taken from vicinity of pillars 1 and 2 for comparison to FEM model.

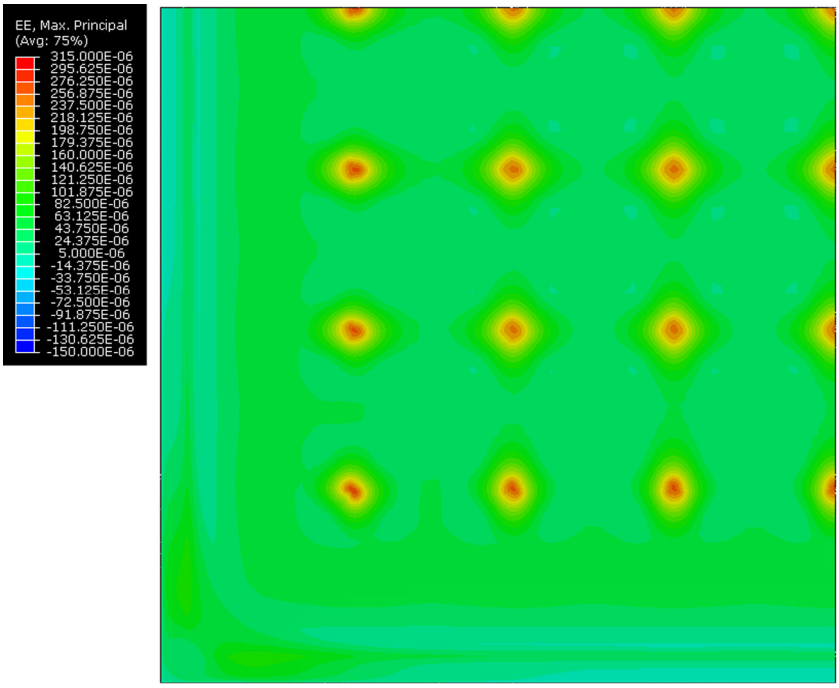


Fig. 11. External glass cover principal strain contours produced via FEM modelling with only atmospheric pressure loading.

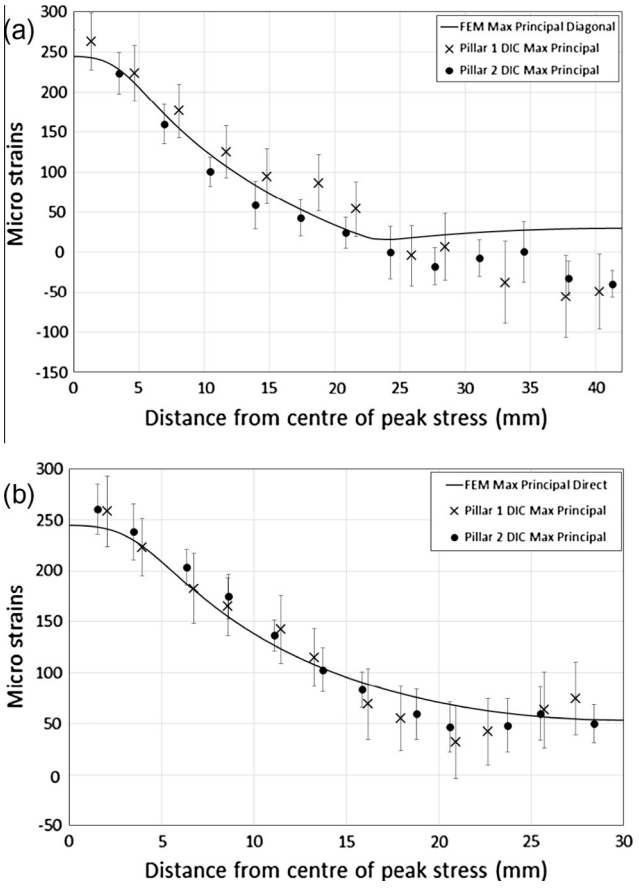


Fig. 12. $\varepsilon_{11}$ strains in the vicinity of a support pillar taken in the (a) diagonal direction and (b) direct direction.

by the DIC were compared with those produced via the FEM simulation (Fig. 4). These strains were consistent with those predicted, see Fig. 12. Error bars in Fig. 12 are determined by the DIC software and are based on the co-variance matrix calculated during the correlation of the digital images. The software utilises an error propagation algorithm that incorporates any image filtering that may have been applied (Thorsten Siebert of Dantec Dynamics, 2015, personal communication).

Figs. 10 and 12 show good agreement between simulation and experiment, with the two sample pillars identified in Fig. 10, being similarly stressed in a manner consistent with FEM predictions. This supported the current FEM modelling approach and lent confidence to further FEM predictions. It was observed that no Hertzian fractures occurred during testing, with the enclosure being evacuated for several hours at a time, this supports the assumption that the pillars are suitably flat and effectively support the glass cover.

### 2.4. FEM modelling of enclosure stress due to differential thermal expansion and atmospheric pressure loading

The FEM analysis of the enclosure was extended to consider the case of the enclosure being 240 °C cooler than the stress free temperature of the solder taking into account differential thermal expansion stresses. Predicted principal stress profiles are reported on the symmetry plane (see thick dotted arrow in Fig. 8b) along the external, internal and inside surfaces of the glass in a similar manner to Fig. 4.

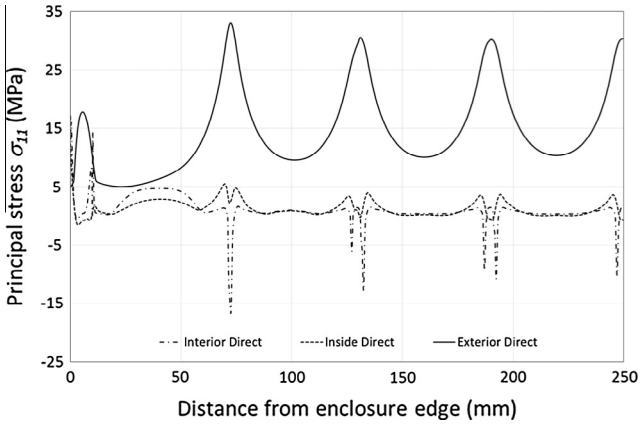


Fig. 13. Principal stress profiles of glass cover for 0.5 $m^2$ enclosure.

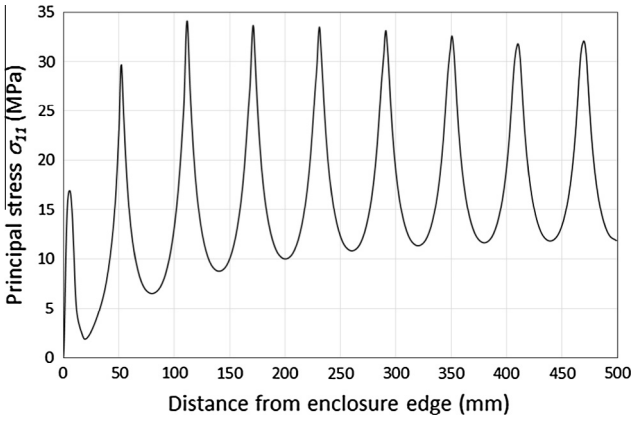


Fig. 15. Principal stress of external glass cover surface for 1 × 1 m enclosure.

The stress components plotted in Fig. 13 illustrate the change in stress due to differential thermal expansion. Peak principal stresses on the external glass surface in the case of only atmospheric pressure loading, as according to Fig. 5 in Section 2.1, were ~22.5 MPa. In Fig. 13 these stresses are observed to increase by 8–12 MPa with the inclusion of differential thermal expansion in extreme winter conditions.

Fig. 14 plots the principal stress contours on the external surface of the glass cover. On inspecting these contours the stress pattern resulting from pillar indentation is visible and appears relatively consistent across the surface within a few mega Pascal. The max stress on this surface in the vicinity of the edge seal is ~25 MPa, as seen in Fig. 14, occurring close to the corner edges of the enclosure.

Even with the inclusion of differential thermal expansion stresses (peaking at 33 MPa) this set of design parameters remains within the desired enclosure constraints and is considered to be suitable for an evacuated flat plate solar collector. The size of enclosure first modelled, Fig. 8, is designed for experimental testing using the DIC system. It is possible to model the stress in larger enclosures with dimensions similar to conventional solar thermal collectors to show whether the local stresses are scale-dependent. A larger FEM quarter geometry, of a 1 $m^2$ vacuum solar collector, was created with the same enclosure component configuration and mesh properties as was used previously. Fig. 15 plots the principal stresses on the external glass cover along a line corresponding to the centre most row of support pillars. The enclosure in this case is seen to be similarly stressed in comparison to Fig. 13 with peak principal stresses of ~33 MPa in the vicinity of the support pillars. The impact of the differential thermal expansion is again seen to increase peak stresses by ~8–12 MPa. It can be seen in Fig. 15 that at between 0.15 and 0.2 m from the enclosure edge the tensile stress peaks with a level similar to the centre of the enclosure. These results suggest that this configuration of enclosure would be suitable for a

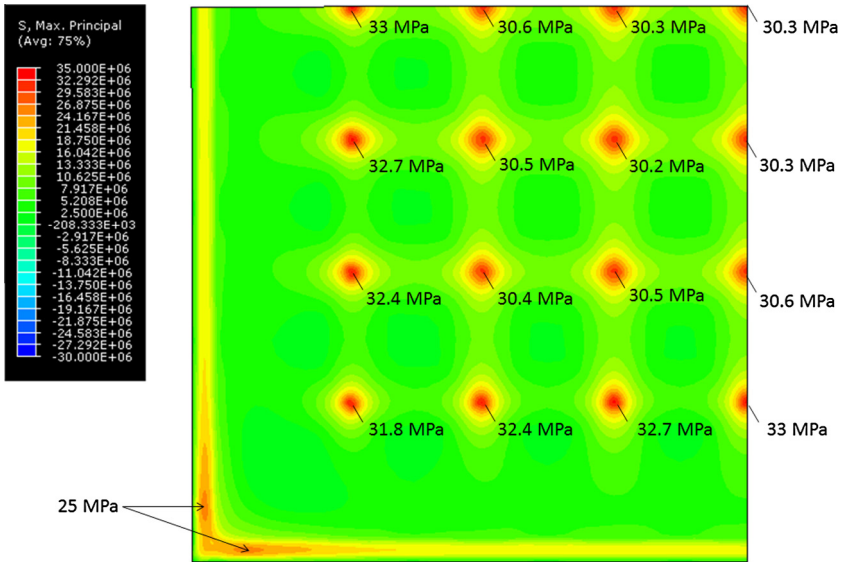


Fig. 14. Principal stress contours on external glass cover surface, enclosure subject to atmospheric pressure loading and differential thermal expansion stresses.

evacuated flat plate solar collector sized similarly to a conventional flat plate system.

## 3. Conclusions

The production of flat plate evacuated solar thermal collectors that will be safe, robust and vacuum-tight for the collector's minimum design lifetime requires a durable vacuum enclosure structure. Any structure assembled from materials with dissimilar expansion coefficients will inevitably experience thermal expansion induced stresses as its temperature changes away from the initial bonding temperature. The enclosure concept identified in this paper experiences some differential expansion stresses; however, it is expected that tempered glass may be easily utilised. With correct selection of enclosure mechanical design parameters this enclosure design should be able to withstand sustained stress due to atmospheric pressure loading and differential thermal expansion resulting from exposure to winter conditions with no damage.

From the finite element analyses the enclosure will be subject to significant and continuous differential thermal expansion stresses, particularly when subjected to winter conditions. Use of metals such as 400 series stainless for the rear collector housing and 4 mm tempered glass for the collector front cover, resulted in acceptable levels of additional thermal stress in the structure. Finite element analysis of a $1 \times 1$ m enclosure with a 4 mm glass cover predicts that tensile stress peaks on the external glass cover in the vicinity of support pillars and levels off to a maximum stress level over a distance of between 0.15 and 0.2 m inwards from the edge. Preliminary experimental measurements of glass cover surface strain were found to be consistent with FEM simulation results. Service conditions for flat panel collectors can include more complex environmental and operational conditions such as wind loading, impacts and transient thermal situations: these were not modelled in the current analysis.

The results of this study however suggest that, with suitable selections of design parameters, this enclosure design will be robust under a wide variety of scenarios and able to effectively provide a vacuum-insulated environment as part of a high-efficiency evacuated flat plate solar collector.

## Acknowledgements

This project was supported by the Engineering and Physical Science Research Council within the High Performance Vacuum Flat Plate Solar Thermal Collector for Hot Water and Process Heat project (EP/K009230/1). Model and experimental data discussed in this work can be found at: https://dx.doi.org/10.17028/rd.lboro.2069672.

## References

Abbott, M., Madocks, J., 2001. Roller wave distortion–definition, causes and a novel approach to accurate, on-line measurement the main text. Glass Process. Days Proc., 18–21

Benz, N., Beikircher, T., 1999. High efficiency evacuated flat-plate solar collector for process steam production. Sol. Energy 65, 111–118.

Collins, R.E., Fischer-Cripps, A.C., 1991. Design of support pillar arrays in flat evacuated windows. Aust. J. Phys. 44, 545–564.

DANTEC-Dynamics, 2014. Q-400 Systems Operation Manual.

Eames, P.C., 2008. Vacuum glazing: current performance and future prospects. Vacuum 82, 717–722. http://dx.doi.org/10.1016/j.vacuum.2007.10.017.

Eaton, C.B., Blum, H.a., 1975. The use of moderate vacuum environments as a means of increasing the collection efficiencies and operating temperatures of flat-plate solar collectors. Sol. Energy 17, 151–158. http://dx.doi.org/10.1016/0038-092X(75)90053-5.

European Committee for Standardisation, 2009. European Standard Draft Norme Européenne. Brussels.

Fischer-Cripps, A.C., Collins, R.E., Turner, G.M., Bezzel, E., 1995. Stresses and fracture probability in evacuated glazing. Build. Environ. 30, 41–59. http://dx.doi.org/10.1016/0360-1323(94)E0032-M.

Langitan, F.B., Lawn, B.R., 1969. Hertzian fracture experiments on abraded glass surfaces as definitive evidence for an energy balance explanation of Auerbach's law. J. Appl. Phys. 40, 4009–4017. http://dx.doi.org/10.1063/1.1657136.

MBR-Electronics, 2009. Active Solder Alloy CERASOLZER [WWW Document]. URL: <http://www.cerasolzer.com/cerasolzer/cerasolzer_gb.html> (accessed 2.18.15).

Moss, R., Shire, S., 2014. Design and Performance of Evacuated Solar Collector Microchannel Plates. EuroSun Conference. Aix-les-Bains, France.

Mouginot, R., Maugis, D., 1985. Fracture indentation beneath flat and spherical punches. J. Mater. Sci. 20, 4354–4376.

Overend, M., Zammit, K., 2012. A computer algorithm for determining the tensile strength of float glass. Eng. Struct. 45, 68–77. http://dx.doi.org/10.1016/j.engstruct.2012.05.039.

S-Bond, 2015. S-Bond Technologies Products [WWW Document]. URL: <http://www.s-bond.com/products/> (accessed 07.27.15).

Schneider, J., Schula, S., Weinhold, W.P., 2012. Characterisation of the scratch resistance of annealed and tempered architectural glass. Thin Solid Films 520, 4190–4198. http://dx.doi.org/10.1016/j.tsf.2011.04.104.

Simko, T.M., Fischer-Cripps, A.C., Collins, R.E., 1998. Temperature-induced stresses in vacuum glazing: modelling and experimental validation. Sol. Energy 63, 1–21.

Vandebroek, M., Belis, J., Louter, C., Van Tendeloo, G., 2012. Experimental validation of edge strength model for glass with polished and cut edge finishing. Eng. Fract. Mech. 96, 480–489. http://dx.doi.org/10.1016/j.engfracmech.2012.08.019.

Wang, J., Eames, P.C., Zhao, J.F., Hyde, T., Fang, Y., 2007. Stresses in vacuum glazing fabricated at low temperature. Sol. Energy Mater. Sol. Cells 91, 290–303. http://dx.doi.org/10.1016/j.solmat.2006.10.007.